Identifying Electromagnetic Noise-Source Impedance Using Hybrid of Measurement and Calculation Method

Feng Zheng, *Member, IEEE*, Wugang Wang, Xiaofan Zhao, Mengke Cui, Qiang Zhang, and Guqing He

***Abstract*—Identifying the noise impedance is a key step to improve the performance of an electromagnetic interference (EMI) filter. This paper proposes an impedance perturbation method to measure and calculate unknowns under a wide frequency range. Not only the differential mode/common mode (DM/CM) impedances but also the magnitude and the phase of impedances will be obtained at the same time. Moreover, the extraneous solution introduced by computation is checked. In addition, the profile of the perturbation infrastructure almost keeps the same under different cases, and it will limit the error of measurement under a very low level, which is also discussed in detail. Finally, the experimental results validate the methods very well.**

***Index Terms*—Electromagnetic interference (EMI) filter, impedance perturbation, noise impedance, scattering parameters.**

I. Introduction

ELECTROMAGNETIC compatibility is an important issue for the electronic systems working safely and reliably. The high *dv*/*dt* and *di*/*dt* electromagnetic pulse will induce power integration or signal integration problems. Nevertheless, as more and more wideband switching components are applied in power electronic systems, the pulse intensity as well as the probability of noises interfering will be dramatically increased [1]–[4]. Hence, a variety of methods are adopted to alleviate these negative impacts, and among them utilizing an electromagnetic interference (EMI) filter to attenuate the noise is still the most preferable one [5]–[9]. Then, how to improve the performance of an EMI filter has become a major concern.

Impedance mismatching is a popular method to improve the performance of an EMI filter. Fully utilizing the mismatching will lead to shrinking of an EMI filter without compromising its

Manuscript received July 27, 2018; revised November 13, 2018; accepted December 23, 2018. Date of publication January 7, 2019; date of current version June 28, 2019. This work was supported by the National Natural Science Foundation of China under Grants 51077106 and 51775404. Recommended for publication by Associate Editor M. Tavakoli Bina. *(Corresponding author: Feng Zheng.)*

F. Zheng, W. Wang, M. Cui, Q. Zhang, and G. He are with the Department of Electrical Engineering, School of Electrical and Mechanical Engineering, Xidian University, Xi'an 710071, China (e-mail:

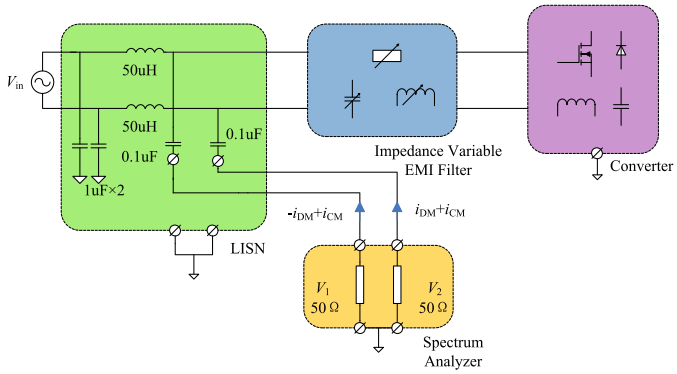

Fig. 1. Block diagram of measurement setup.

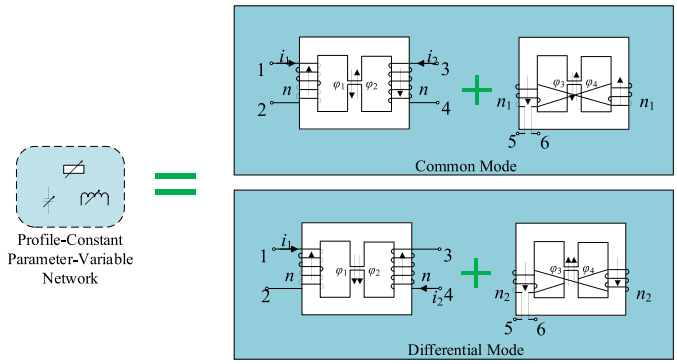

Fig. 2. Profile-constant parameter-variable network.

accuracy, and ease of operation. After weighing all of these factors, we proposed an IL perturbation method, which can be considered as expansion of the *I–V* method, to measure the impedance of a noise source.

This paper presents a method that inserting an EMI filter with variable impedance and noise response is measured at the same time, as shown in Fig. 1. Then, a series of calculation by deducing the scattering parameters (*s*-parameters) was used to obtain the CM and DM noise source impedances, respectively. It adopts a profile-constant parameter-variable network (PCPVN) to achieve impedance perturbations in a wider frequency band, as shown in Fig. 2. Meanwhile, the errors and applicable conditions are analyzed under different numerical examples in this paper. Therefore, designers can flexibly use this method to recognize the impedance of the noise source accurately, and impedance mismatching is achieved as much as possible.

This paper is organized as follows. Sections II and III provide the methodology for measurements; Section IV is the experimental verification; and discussion and conclusions are presented in Sections V and VI, respectively.

II. Methodology for Measurements

The principle of the measurement is quite simple. Since the noise level read by the spectrum analyzer is closely related to the amplitude and impedance of the noise source as well as the EMI filter, we can describe the relationship by forming an equation. Assuming the noise source keeps almost constant during the measurement procedure and the character of EMI filters is exactly known, a series of equations on the impedance of noise source will be obtained by varying the character of EMI filters. Finally, the impedance will be gotten by solving these equations.

A. Obtaining the Simultaneous Equations for Impedance Calculation

The IL of EMI filters is an important index to characterize their suppression capabilities, and IL can be defined in different forms based on various kinds of parameters. *s*-Parameters are popularly used thanks to their simplicity, accuracy, and easy implementation [24]–[26]. The typical IL of a two-port network can be defined as the following form in terms of *s*-parameters [27]:

$$\begin{aligned} \mathrm{IL} &= 20 \cdot \lg \left| \frac{(1-S_{11}\Gamma_S)(1-S_{22}\Gamma_L)-S_{21}\Gamma_L S_{12}\Gamma_S}{S_{21}(1-\Gamma_L\Gamma_S)} \right| \\ &= 20 \log \left| \frac{V_{20}}{V_2} \right| \end{aligned} \tag{1}$$

where V_{20} is the voltage across line impedance stabilization network (LISN) without a filter, whereas V_2 is the voltage after the filter being applied, and the reflection coefficients on load side (Γ_L) and noise source side (Γ_S) are defined as

$$\Gamma_L = \frac{z_L - z_0}{z_L + z_0},\ \Gamma_s = \frac{z_s - z_0}{z_s + z_0}.$$

For simplifying the calculation, attenuation capability is described in a nonlogarithm form as

$$I = \left| \frac{(1-S_{11}\Gamma_S)(1-S_{22}\Gamma_L)-S_{21}\Gamma_L S_{12}\Gamma_S}{S_{21}(1-\Gamma_L\Gamma_S)} \right| = \left| \frac{V_{20}}{V_2} \right|. \tag{2}$$

It is well known that the equivalent load impedance in common and differential mode is 25 and 100 Ω, respectively [27], [28]. Hence, the corresponding Γ_L equals to 1/3 and –1/3, respectively. Then, (2) in the common mode can be simplified as

$$I = \left| \frac{\Delta}{S_{21}} + \frac{3 - S_{22} - 3\Delta}{S_{21}} \frac{1}{(3-\Gamma_S)} \right| \tag{3}$$

where

$$\Delta = 3S_{11} - S_{11}S_{22} + S_{21}S_{12}$$

and let

$$\vec{x} = \frac{1}{3-\Gamma_S}, \vec{a} = \frac{\Delta}{3 - S_{22} - 3\Delta}, \text{ and } c = \left| \frac{S_{21}}{3 - S_{22} - 3\Delta} \right| I. \tag{4}$$

Substituting these two vectors $\vec{x}$ and $\vec{a}$ and variable c into (3) will lead to

$$c = |\vec{a} + \vec{x}|. \tag{5}$$

Expanding (5), we will get

$$\vec{a}\vec{a}^* + \vec{a}^*\vec{x} + \vec{a}\vec{x}^* + \vec{x}\vec{x}^* = c^2 \tag{6}$$

where

$$c^2 = \left|\frac{S_{21}}{1 - S_{22} - \Delta}\right|^2 I^2 = \left|\frac{S_{21}}{1 - S_{22} - \Delta}\right|^2 \frac{V_{20}^2}{V_2^2}$$

Now, we set $\vec{x} = u + jv$, and substituting $\vec{x}$ into (6) yield

$$\vec{a}\vec{a}^* + \vec{a}^* (u + jv) + \vec{a} (u - jv) + u^2 + v^2 = c^2. \quad (7)$$

Since the noise signal V_2 can be measured, we can write

$$d = \vec{a}\vec{a}^*,\ f = \vec{a}^* + \vec{a},\ e = j (\vec{a}^* - \vec{a}),$$

$$g = \frac{1}{V_2^2}\left|\frac{S_{21}}{1 - S_{22} - \Delta}\right|^2.$$

Then, we will get

$$d + fu + ev + u^2 + v^2 = gV_{20}^2. \quad (8)$$

Obviously, (8) involves three unknowns, namely, *u*, *v*, and V_{20}^2, where *u* and *v* are closely related to the noise impedance, and V_{20} is the noise source voltage. If these unknowns are obtained, the noise impedance will be gotten. Thus, we must setup a set of simultaneous equations (SE) as demonstrated in the following equation:

$$\begin{cases} d_1 + f_1 u + e_1 v + u^2 + v^2 = g_1 V_{20}^2 \\ d_2 + f_2 u + e_2 v + u^2 + v^2 = g_2 V_{20}^2 \\ d_3 + f_3 u + e_3 v + u^2 + v^2 = g_3 V_{20}^2. \end{cases} \quad (9)$$

After solving (9), we will get the CM impedance of the power supply. Similarly, DM noise impedance of the power supply can be obtained following the identical procedure.

B. Formulating SE With PCPVN

The straightforward method of formulating SE's is to measure the noise level across LISN under different cases while keep the noise source and its impedance constant. Therefore, we need three different two-port networks to obtain three sets of *s*-parameters. Generally speaking, variations in components' value will derive different *s*-parameters. However, the change of components' value will bring variations in profile, and the difference may be bigger when the changes take place on inductors or capacitors.

In order to maintain the same working condition for power supply, we must reduce the impact introduced by different experimental setup as small as possible. In other words, the coupling effects, such as mutual inductance and capacitances among components of the power supply and EMI filters, should practically keep constant under various measurements. Hence, we fabricate a PCPVN using an integrated magnetic component to fulfill this task. As shown in Fig. 2, the integrated magnetic component is wound with a tunable port, which we named balance winding. Then, the two port *s*-parameters will be varied by connecting different tiny profile components to the tunable port. Since the component size is so small, the impact on the coupling path will be negligible.

We theoretically explain PCPVN's working principle in terms of six-port network parameter, as shown in Fig. 2. Taking the frame of the power supply as the common ground, we can then regard the PCPVN as a six-port network S_{6*6}. Ports 1, 2, 3, and 4 comprise the power path, whereas ports 5 and 6 are two leading-out ports of the balanced winding. The balanced impedance is connected across leads 5 and 6. Then the six-port network is converted into four-port network, the *s*-parameters of the four-port network are S'_{4*4}, and it will be changed when different balanced impedance is connected. At the same time, the filtering characteristic of the integrated magnetic component will be varied significantly.

The PCPVN's IL in CM and DM will be derived with respect to the four-port mix-mode network. Following *s*-parameter theories, we will obtain a four-port network after a two-port network being cascaded down to a six-port network, and the relationships among incidental and reflected waves on the network ports will then be described as follows:

$$[b]_{1*8} = \begin{bmatrix} S_{6*6} & 0 \\ 0 & S_{2*2} \end{bmatrix} [a]_{1*8} \quad (10)$$

where the S_{2*2} is parameters of the two-port network. The *s*-parameter matrix in (10) can be divided into a set of submatrices by rearranging its elements. The rearranging rule is that the *s*-parameters of the unconnected ports are collected together and left the *s*-parameters of the connected ports together. The full matrix is then comprised of four 4×4 subblocks, as shown in the following equation:

$$[b]_{1*8} = \begin{bmatrix} S_{I-I} & S_{I-\mathrm{II}} \\ S_{\mathrm{II}-I} & S_{\mathrm{II}-\mathrm{II}} \end{bmatrix} [a]_{1*8} \quad (11)$$

where $S_{\mathrm{I}-\mathrm{I}}$, $S_{\mathrm{I}-\mathrm{II}}$, $S_{\mathrm{II}-\mathrm{I}}$, and $S_{\mathrm{II}-\mathrm{II}}$ are the four submatrix. Hence, we will get the mix-mode *s*-parameters of the four-port PCPVN based on the relationship among ports as following:

$$[S]'_{4*4} = [S_{I-I}] + [S_{I-\mathrm{II}}] \left([\varepsilon] - [S_{\mathrm{II}-\mathrm{II}}]\right)^{-1} [S_{\mathrm{II}-\mathrm{I}}] \quad (12)$$

where $[\varepsilon]$ is called the connection matrix

$$[\varepsilon] = \begin{bmatrix} 0 & 0 & 0 & 1 \\ 0 & 0 & 1 & 0 \\ 0 & 1 & 0 & 0 \\ 1 & 0 & 0 & 0 \end{bmatrix}.$$

Clearly, the mix-mode *s*-parameters involve both CM and DM information, and the functionality of the DM and CM noise attenuation can be described by 2 two-port networks, respectively [27], [29]. Then, following the rule of transforming a four-port to a two-port matrix yield

$$[S]'_{4*4} = [B] [S'] [A]^{-1} = \begin{bmatrix} S_{cc} & S_{cd} \\ S_{dc} & S_{dd} \end{bmatrix} \quad (13)$$

where

$$[A] = [B] = \frac{1}{\sqrt{2}} \begin{bmatrix} 1 & 1 & 0 & 0 \\ 1 & 1 & 0 & 0 \\ 0 & 0 & 1 & 1 \\ 0 & 0 & 1 & 1 \end{bmatrix}.$$

The S_{cc} submatrix contains the CM *s*-parameters, which is related to the *s*-parameters of the new two-port CM filter as follows:

$$S_{cc} = \begin{bmatrix} S_{cc11} & S_{cc12} \\ S_{cc21} & S_{cc22} \end{bmatrix} = \frac{1}{2}\begin{bmatrix} S'_{11}+S'_{13}+S'_{31}+S'_{33} & S'_{12}+S'_{14}+S'_{32}+S'_{34} \\ S'_{21}+S'_{23}+S'_{41}+S'_{43} & S'_{22}+S'_{24}+S'_{42}+S'_{44} \end{bmatrix}. \tag{14}$$

The S_{dd} submatrix contains the DM *s*-parameters, which is related to the *s*-parameters of the new two-port DM filter as follows:

$$S_{dd} = \begin{bmatrix} S_{dd11} & S_{dd12} \\ S_{dd21} & S_{dd22} \end{bmatrix} = \frac{1}{2}\begin{bmatrix} S'_{11}-S'_{13}-S'_{31}+S'_{33} & S'_{12}-S'_{14}-S'_{32}+S'_{34} \\ S'_{21}-S'_{23}-S'_{41}+S'_{43} & S'_{22}-S'_{24}-S'_{42}+S'_{44} \end{bmatrix}. \tag{15}$$

According to (12)–(15), we can obtain the CM and DM *s*-parameters. It is readily seen from (11) and (12) that the parameters of two-port network will change when different balanced impedances are connected across ports 5 and 6.

III. Determination of Real Value by Hybrid of Measurement and Calculation Method

Calculation or verification of the obtained solutions is an essential step to acquire the noise impedance. As shown in (9), the SEs are all second-order equations. Typically, there will be two solutions for every unknown. However, IL has just a certain value when the noise source is kept constant. Obviously, we have to determine which one is the real result, namely the real noise source impedance.

Since the three unknowns *u*, *v*, and V_{20} are all needed to be tested, it is difficult to fulfill the trial just by measurements. V_{20} is superficially the one might be measured. Nevertheless, noise level on the LISN is so high in case of no EMI filter being applied that it may be over the input range of an instrument. Thus, we measure the noise voltage on the load side with an EMI filter being connected instead. Assume V_2^1 and V_2^2 are the noise voltages across the LISN when two different filters are applied, and the right side of (2) will be calculated using the measured *s*-parameter and noise source impedance to be trialed, and the results are

$$\begin{aligned} I_1 &= \left| \frac{(1-S_{11}^1\Gamma_S)(1-S_{22}^1\Gamma_L)-S_{21}^1\Gamma_L S_{12}^1\Gamma_S}{S_{21}^1(1-\Gamma_L\Gamma_S)} \right| \\ I_2 &= \left| \frac{(1-S_{11}^2\Gamma_S)(1-S_{22}^2\Gamma_L)-S_{21}^2\Gamma_L S_{12}^2\Gamma_S}{S_{21}^2(1-\Gamma_L\Gamma_S)} \right|. \end{aligned} \tag{16}$$

According to (2), we can get

$$\begin{aligned} I_1 &= \frac{V_{20}}{V_2^1} \\ I_2 &= \frac{V_{20}}{V_2^2}. \end{aligned} \tag{17}$$

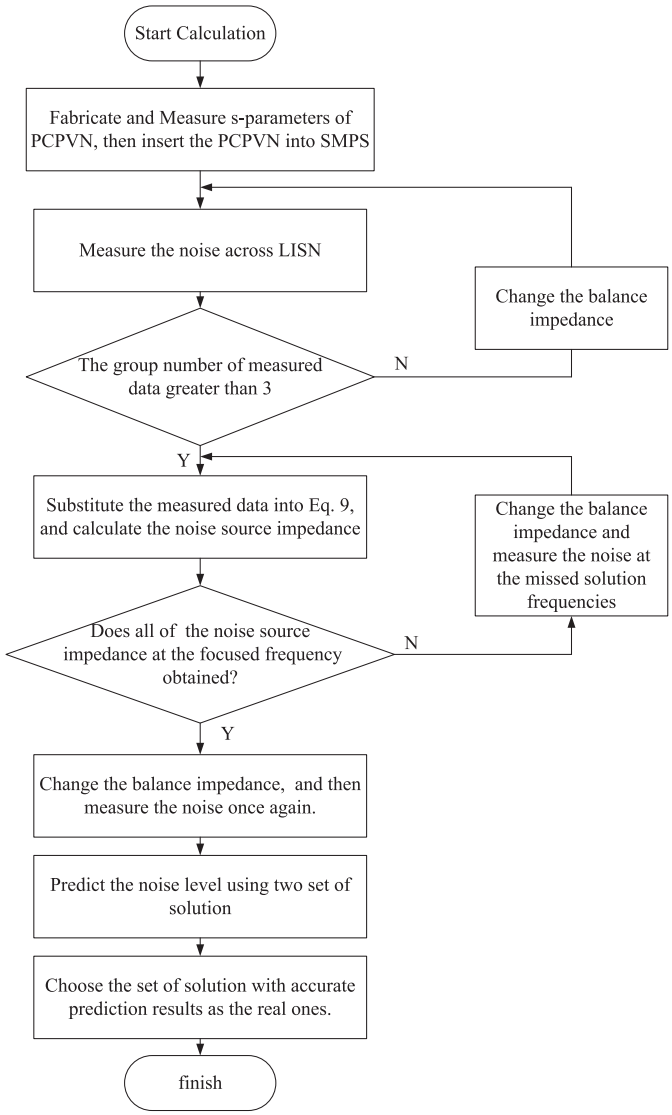

Fig. 3. Flowchart of our methodology.

Further simplification leads to

$$V_2^2 = \frac{I_1}{I_2} V_2^1. \tag{18}$$

Because we have gotten two sets of noise source impedance, two IL can be obtained. Then, we will obtain two calculated V_2^2 using (18), and compare the calculated V_2^2's with the measured one. Finally, the impedance corresponding to the equaling result is the real set of noise source impedance.

A. Measurement Step Summary

Identifying the noise source impedance should follow the steps shown in Fig. 3. Although the procedures seem complex, designers will obtain all his or her focused noise impedance. Owing to the accuracy of *s*-parameters spanned over a wide frequency, the measurement will also keep almost the same accuracy all over the CISPR22 demand frequency range. Moreover, if perturbation plays no effect at some frequencies, we

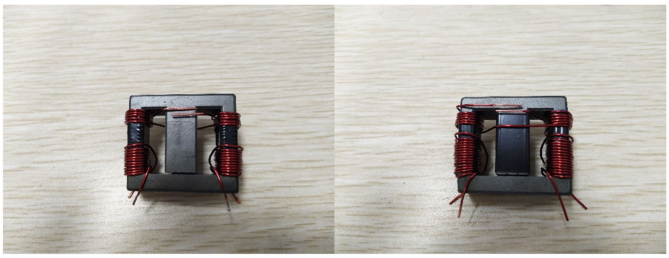

Fig. 4. CM inductor with balanced winding.

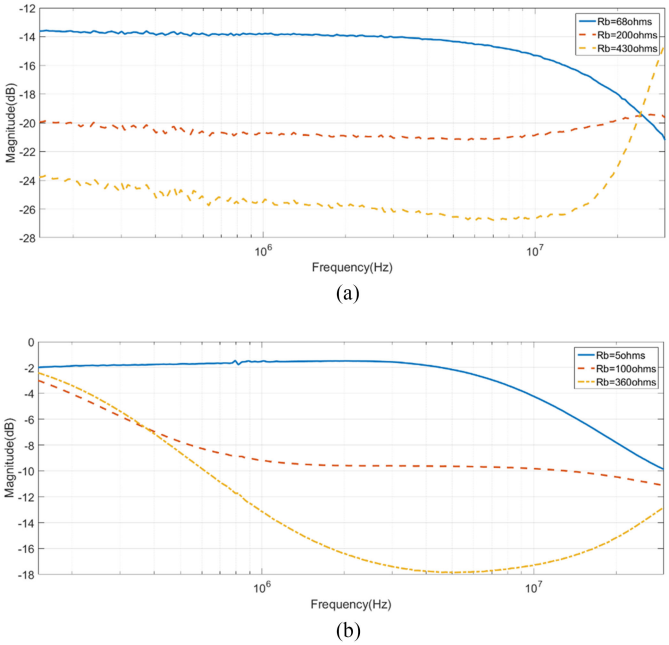

Fig. 5. Comparison of IL. (a) Comparison of CM IL. (b) Comparison of DM IL.

only need to accumulate the data on these missed solution frequencies. Thus, the method will present solutions on all cared frequencies and reduce the work to a very low level.

IV. Experimental Results

A. Measurement of the s-Parameter

A photograph of the CM inductor with balanced winding is shown in Fig. 4. The central leg of the E-E core is provided with air-gap. In experimental setup, the balanced impedance we choose to be connected across ports 5 and 6 is 68, 200, 430, 5, 100, and 360 Ω, respectively. The CM and DM IL of the integrated magnetic element will be changed when different impedances are connected, and the results are shown in Fig. 5.

B. Calculation of CM Noise Source Impedance

The calculation of CM noise impedance is carried out in the first step. The experimental setup contains a two-port LISN and a 0° power combiner, which is used to separate the noise, as shown in Fig. 6 [30], 31]. The output of the power combiner is the sum of the noise signal of the light and neutral line, and it is

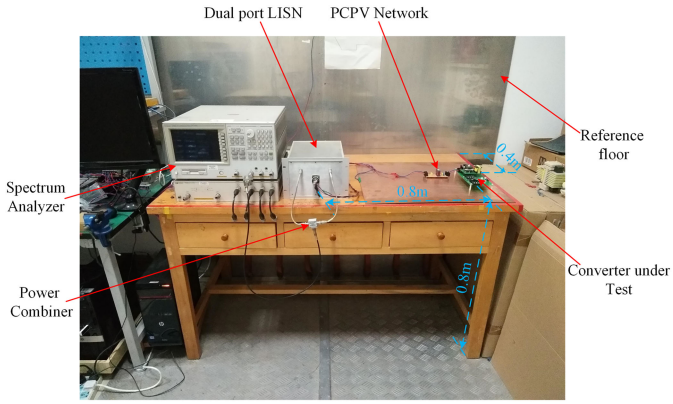

Fig. 6. Picture of the experimental setup.

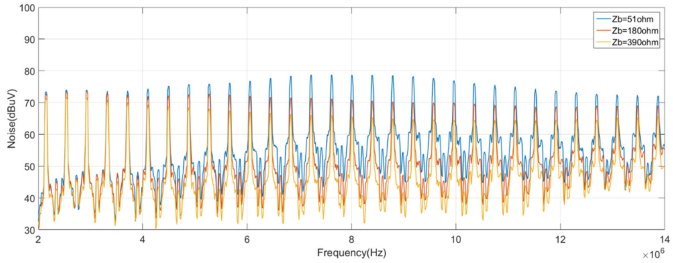

Fig. 7. CM noise when different resisters were connected between port 5 and 6.

two times higher than the actual CM noise. Therefore, the final measured results minus 6 dB are the real CM noise. In order to reduce the coupling effects between the noise source and the integrated magnetic element, the integrated magnetic element is covered by an iron box, and we can regard it as a black box system. A series of impedances are sequentially connected across ports 5 and 6 to change the *s*-parameters of the black box. Thus, the CM IL of the black box is changed following these impedances.

The power supply to be measured is a voltage-source inverter, and its input voltage is 60 V. Generally, the CM noise is mainly located in the frequency range from 2 to 10 MHz. The measured results are shown in Fig. 7, where three different balanced impedances are sequentially connected across port 5 and port 6.

The CM noise source impedance is obtained by aligning the SE's and solving them. The magnitude and phase of the CM impedance are calculated and are shown in Figs. 7 and 8. As aforementioned, there is only one solution that is the real, although two solutions are displayed. Then, we will verify the real solution in the next step.

C. Verification of the Correctness of the Solution

We applied two extra integrated elements to distinguish the real noise source impedance. When a 10-Ω resistor is connected across ports 5 and 6 of the first integrated element, we can measure the noise level on LISN by the spectrum analyzer. Following (16)–(18), we can predict the noise across LISN when a balanced impedance whose value is 82 Ω is connected across

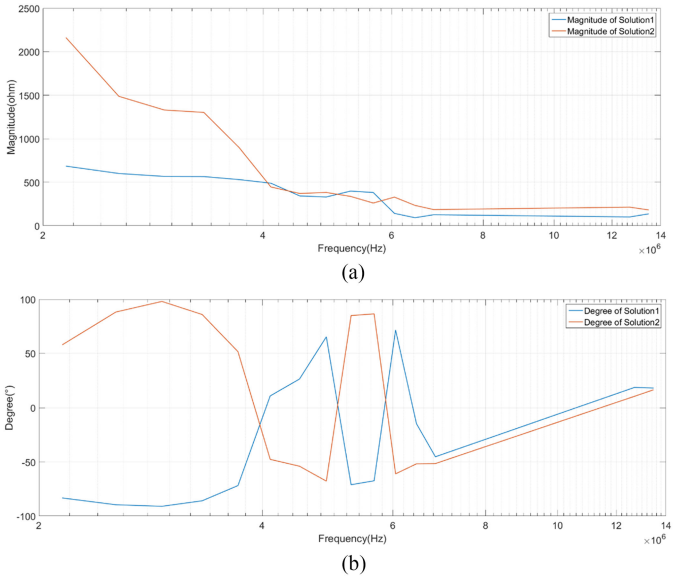

Fig. 8. Calculated result of CM noise source impedance. (a) Magnitude. (b) Phase.

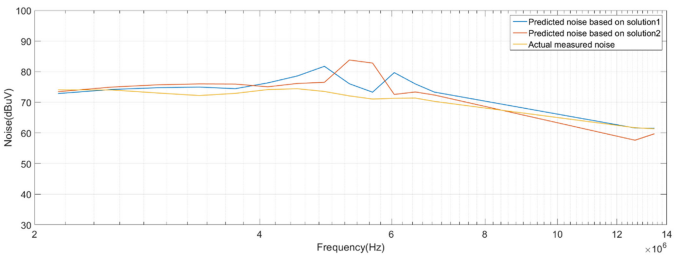

Fig. 9. Comparison of predicted and measured noise.

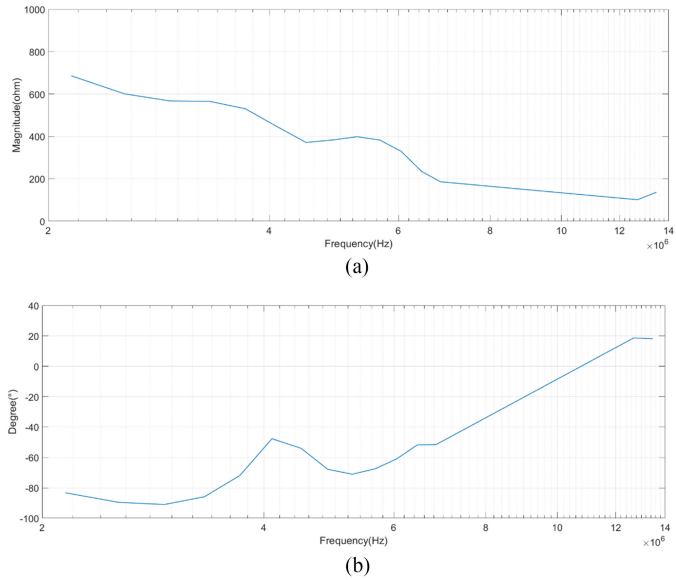

Fig. 10. (a) Magnitude and (b) phase of the real noise source impedance.

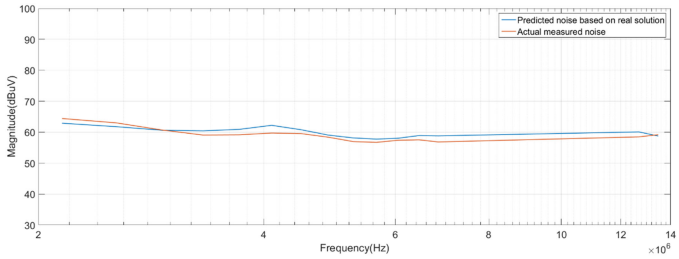

Fig. 11. Comparison of noise after a standard filter inserted between prediction and actual measurement.

ports 5 and 6 of the second integrated element. We can then obtain the CM noise using the aforementioned comparison method, and the results are shown in Figs. 9 and 10.

A commercial EMI filter was used to validate the calculated impedance. At the first step, we obtained the four-port mix-mode *s*-parameter of the filter by measurement. We then calculated the equivalent two-port CM and DM IL, respectively. Thus, we can get the IL based on our calculated impedance, and the noise level across LISN will be predicted. The predicted noise level and measured noise level across LISN are shown in Fig. 11. Obviously, the differences between the two results are so small that we can neglect the error. In other words, the effectiveness of the method is validated.

D. Obtaining DM Noise Source Impedance

The experimental procedures and setup for DM measurement are almost identical to the CM's except a 180° power combiner being used [30], [31]. Because of the large input filter capacitor, the equivalent DM noise source impedance is very small. Hence, our proposed method may yield some inaccurate results. In order to prove the effectiveness of the proposed method, a DM conductor is in series on the input side of the converter, which is used to increasing the DM impedance deliberately. Now the magnitude of the measured impedance should be almost equal to the value of the inductor in series, and the phase of the measured impedance should be close to 90°. The calculated and measured results are shown in Fig. 12, and the negligible difference read from figures validate the effectiveness of the proposed method once again.

V. Dicussion

A. Error Propagation Analysis

Because of the impacts of various factors, such as the precision of the measuring instrument, the measuring condition, and the measuring method, the data obtained from the measurement often have some errors, and the results derived from the inaccurate data will also have some errors, which are named indirect error. Based on the results of the previous experiments, we can see that the value of both the noise prediction and the impedance prediction is in slight difference to the actual measurements. This is because in the case of experiment, the noise source impedance is calculated by measuring the relevant data, namely, *s*-parameters and noise level. In the process of measuring the *s*-parameters and noise, the measurement result has errors due to the inaccuracy of instruments. Thus, the error of

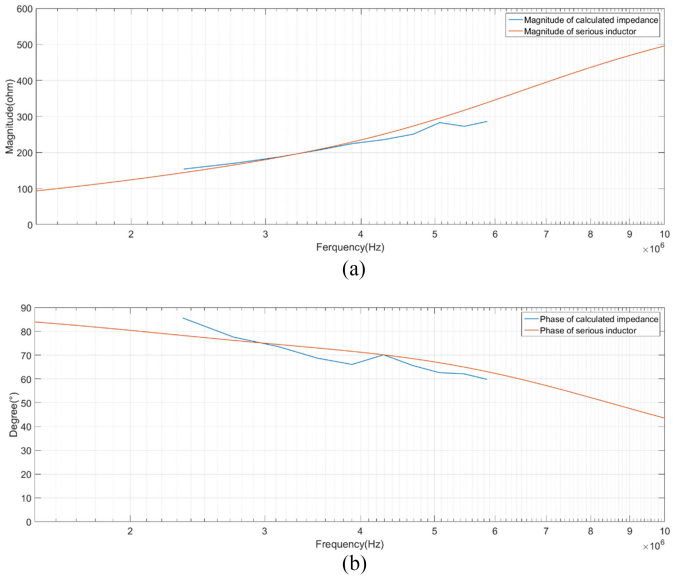

Fig. 12. Comparison between calculated impedance and serious inductor. (a) Magnitude. (b) Phase.

the calculated results may be worsened or may be improved with respect to the weight of the factors. In order to evaluate the reliability of the final results, we need to analyze the cause and the value of the error.

According to (1) we can see that the independent variables are $S_{11}, S_{12}, S_{21}, S_{22}, V_2$, and Γ_S, where Γ_S is a variable associated with the noise source impedance Z_S

$$Z_S = \frac{1-\Gamma_S}{1+\Gamma_S}. \tag{19}$$

Therefore, (19) is alternatively described as

$$Z_S = F\left(S_{11}, S_{12}, S_{21}, S_{22}, V_2\right) \tag{20}$$

where F represents the error propagation function in terms of s-parameters and the noise level.

The errors propagated in the CM calculation procedure are first analyzed. The s-parameter and noise on certain frequency are selected, and we define them as $S'_{11}, S'_{12}, S'_{21}, S'_{22}$, and V'_2. We can then obtain a Z'_S based on these parameters. The error syntheses will be conducted on a typical procedure, and we take S_{11} as an example to demonstrate the procedure. Assume S_{11} contains 5% error, we can obtain a Z''_S by substituting 0.95 S'_{11} to (20) while keep the other four variables unchanged. Thus, the final relative error caused by the measurement error of S_{11} is

$$e_{s11} = \left|\frac{Z'_S - Z''_S}{Z'_s}\right|. \tag{21}$$

Assume that all variables contain 5% error, similarly, the relative error caused by the measurement error of the other four independent variables can also be obtained, namely $e_{s12}, e_{s21}, e_{s22}$, and e_{V2}. Comparing the sum of $e_{s11}, e_{s12}, e_{s21}, e_{s22}$ with e_{V2}, we can know whether the measurement error of the s-parameter or the measurement error of the noise has a greater effect on the result.

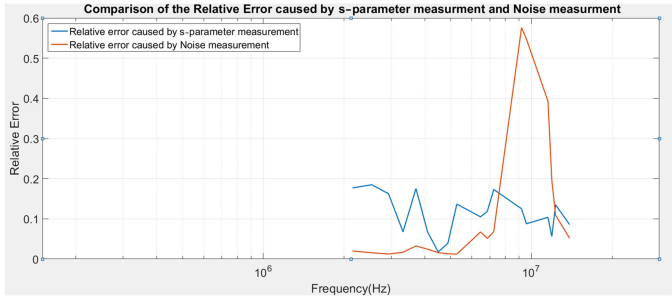

Fig. 13. Comparison of the relative error caused by s-parameter measurement and noise measurement.

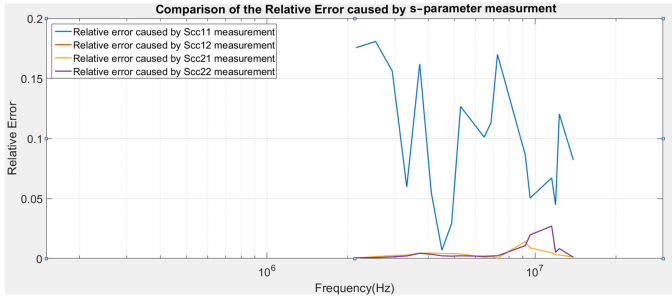

Fig. 14. Comparison of the relative error caused by s-parameter measurement.

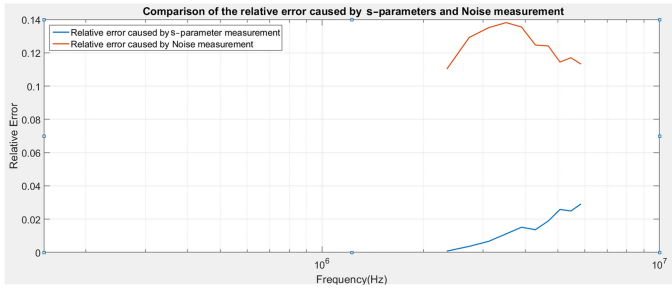

Fig. 15. Comparison of the relative error caused by s-parameter measurement and noise measurement.

The analysis results on error propagation in the case of common mode are shown in Figs. 13 and 14. It can be readily read that the error propagation is more severe when the noise measurement contains inaccuracy, and the uncertainty of S_{cc11} will incur larger error among others. Thus, much attention should be paid and careful calibration should be conducted during the measurement of these sensitive parameters.

The DM error analysis is conducted in the same way. As shown in Fig. 15, the influence of noise measurement error is much larger than that of s-parameters. Furthermore, we can see that the relative error caused by the measurement error of s-parameters is very small. Therefore, we do not have to weigh the impact of differential mode s-parameters.

B. Method Applicability and Improvement

We need to analyze the applicability of the method and put forward improvements to reduce the inaccuracy of the results.

Generally speaking, the common-mode impedance of the voltage-source inverter is large, whereas the counterpart of the differential mode impedance is small. The common-mode noise source impedance calculated by the proposed method is hence more accurate than that of the differential-mode impedance. When a filter inductor is cascaded to alleviate the input current ripple, the proposed method can be used to calculate the differential-mode impedance accurately. The conclusion is that the larger the impedance is, the more accurate the results are.

From the analysis results, we can see that the measurement error of *s*-parameters has little effect on the results obtained in the case of the differential mode. Therefore, we just need to ensure the accuracy of the noise measurement, and then the results will narrow the results' standard deviation. In the case of common mode, we should improve the accuracy not only of noise measurement but also of s_{11}. Furthermore, we must pay attention to that s_{11} is only a description parameter of the equivalent two-port network and is not measured directly. In the experiment, we directly measure the *s*-parameters of the six-port networks. According to (12)–(14), we can obtain

$$\begin{aligned} S_{CC11} &= F'\left(S'_{11}, S'_{13}, S'_{31}, S'_{33}\right) \\ &= F\left(S_{15}, S_{16}, S_{35}, S_{36}, S_{51}, S_{53}, S_{55}, S_{56}, S_{61}, S_{63}, S_{65}, S_{66}\right). \end{aligned} \tag{22}$$

It can be seen clearly from (22) that the equivalent s_{11} is related to the *s*-parameters among ports 1, 3, 5, and 6. Thus, one should take some measures, such as averaging data, carefully calibrating the instruments to improve the accuracy of the *s*-parameters among the four ports.

VI. Conclusion

In this paper, a method is proposed to obtain the CM and DM noise source impedance separately. Compared with conventional ones, the proposed method can accurately obtain the noise source impedance within a wide frequency range. At the same time, the perturbation components are so tiny that the impedance measurement setup is almost under working condition. Hence, the variation and uncertainty in measurement results from setup to prototype are limited to a low level. Moreover, the multiple impedance solution problems are highlighted, and the discussion on the accuracy of measurement consolidates the usefulness of the method. Finally, the results of experiments strongly validate the proposed method.

Appendix

A. Derivation of Analytical Solution

For easier understanding, the concrete process of deriving the analytical solution is given. In other words, the process is that how do we solve (9). We make

$$\begin{aligned} h &= \left(g_3 - g_1\right)\left(g_2 d_1 - g_1 d_2\right) - \left(g_2 - g_1\right)\left(g_3 d_1 - g_1 d_3\right) \\ k &= \left(g_3 - g_1\right)\left(g_2 f_1 - g_1 f_2\right) - \left(g_2 - g_1\right)\left(g_3 f_1 - g_1 f_3\right) \\ l &= \left(g_3 - g_1\right)\left(g_2 e_1 - g_1 e_2\right) - \left(g_2 - g_1\right)\left(g_3 e_1 - g_1 e_3\right). \end{aligned}$$

By using the elimination method, we will get a binary liner equation, as shown in the following

$$h + ku + lv = 0.$$

Meanwhile, we make

$$\begin{aligned} m &= \left(g_2 - g_1\right)\frac{k^2 + l^2}{l^2} \\ n &= \left(g_2 f_1 - g_1 f_2\right) - \frac{k}{l}\left(g_2 e_1 - g_1 e_2\right) + 2\frac{kh}{l^2}\left(g_2 - g_1\right) \\ o &= \left(g_2 d_1 - g_1 d_2\right) - \frac{h}{l}\left(g_2 e_1 - g_1 e_2\right) + \frac{h^2}{l^2}\left(g_2 - g_1\right). \end{aligned}$$

Then, we can get a quadratic equation with one unknown

$$mu^2 + nu + o = 0. \tag{23}$$

After solving the equation, we get

$$\begin{aligned} u_1 &= \frac{-n + \sqrt{n^2 - 4mo}}{2m} \\ u_2 &= \frac{-n - \sqrt{n^2 - 4mo}}{2m}. \end{aligned} \tag{24}$$

Therefore, we obtain two $\vec{x}$, as shown below

$$\begin{aligned} \vec{x}_1 &= u_1 + jv_1 \\ \vec{x}_2 &= u_2 + jv_2. \end{aligned} \tag{25}$$

According to (4), (19), (24), and (25), the CM noise impedance can be obtained

$$\begin{aligned} z_{\mathrm{scm}1} &= \frac{1 - 4\left(u_1 + jv_1\right)}{4\left(u_1 + jv_1\right) - 2} \\ z_{\mathrm{scm}2} &= \frac{1 - 4\left(u_2 + jv_2\right)}{4\left(u_2 + jv_2\right) - 2}. \end{aligned} \tag{26}$$

Similarly, DM noise impedance of the power supply can be obtained following the identical procedure.

B. Implementation of Two-Port Network

As aforementioned, the two-port network *s*-parameters are derived from the six-port network *s*-parameters. The scatter parameter of six-port network is

$$\mathbf{S} = \begin{bmatrix} S_{11} & S_{12} & S_{13} & S_{14} & S_{15} & S_{16} \\ S_{21} & S_{22} & S_{23} & S_{24} & S_{25} & S_{26} \\ S_{31} & S_{32} & S_{33} & S_{34} & S_{35} & S_{36} \\ S_{41} & S_{42} & S_{43} & S_{44} & S_{45} & S_{46} \\ S_{51} & S_{52} & S_{53} & S_{54} & S_{55} & S_{56} \\ S_{61} & S_{62} & S_{63} & S_{64} & S_{65} & S_{66} \end{bmatrix}. \tag{27}$$

Let

$$[S_{II}] = \begin{bmatrix} S_{11} & S_{12} & S_{13} & S_{14} \\ S_{21} & S_{22} & S_{23} & S_{24} \\ S_{31} & S_{32} & S_{33} & S_{34} \\ S_{41} & S_{42} & S_{43} & S_{44} \end{bmatrix} [S_{I\amalg}] = \begin{bmatrix} S_{15} & S_{16} & 0 & 0 \\ S_{25} & S_{26} & 0 & 0 \\ S_{35} & S_{36} & 0 & 0 \\ S_{45} & S_{46} & 0 & 0 \end{bmatrix}$$

$$[S_{\amalg I}] = \begin{bmatrix} S_{51} & S_{52} & S_{53} & S_{54} \\ S_{61} & S_{62} & S_{63} & S_{64} \\ 0 & 0 & 0 & 0 \\ 0 & 0 & 0 & 0 \end{bmatrix} [S_{\amalg\amalg}] = \begin{bmatrix} S_{55} & S_{56} & 0 & 0 \\ S_{65} & S_{66} & 0 & 0 \\ 0 & 0 & S_{77} & S_{78} \\ 0 & 0 & S_{87} & S_{88} \end{bmatrix}$$

$$[\varepsilon] = \begin{bmatrix} 0 & 0 & 0 & 1 \\ 0 & 0 & 1 & 0 \\ 0 & 1 & 0 & 0 \\ 1 & 0 & 0 & 0 \end{bmatrix}.$$

Then, the scatter parameters of this new four-port network are

$$[S]' = \begin{bmatrix} S'_{11} & S'_{12} & S'_{13} & S'_{14} \\ S'_{21} & S'_{22} & S'_{23} & S'_{24} \\ S'_{31} & S'_{32} & S'_{33} & S'_{34} \\ S'_{41} & S'_{42} & S'_{43} & S'_{44} \end{bmatrix}$$
$$= [S_{II}] + [S_{I\amalg}] \left([\varepsilon] - [S_{\amalg\amalg}]\right)^{-1} [S_{\amalg I}]. \quad (28)$$

Afterward, the equivalent two-port network *s*-parameters can be obtained by (12)–(14)

$$S' = \begin{bmatrix} s_{51} - \sigma_4 s_{15} - \sigma_8 s_{16} & s_{52} - \sigma_3 s_{15} - \sigma_7 s_{16} \\ s_{61} - \sigma_4 s_{25} - \sigma_8 s_{26} & s_{62} - \sigma_3 s_{25} - \sigma_7 s_{26} \\ -\sigma_8 s_{36} - \sigma_4 s_{35} & -\sigma_7 s_{36} - \sigma_3 s_{35} \\ -\sigma_8 s_{46} - \sigma_4 s_{45} & -\sigma_7 s_{46} - \sigma_3 s_{45} \end{bmatrix}$$
$$\begin{bmatrix} s_{53} - \sigma_2 s_{15} - \sigma_6 s_{16} & s_{54} - \sigma_1 s_{15} - \sigma_5 s_{16} \\ s_{63} - \sigma_2 s_{25} - \sigma_6 s_{26} & s_{64} - \sigma_1 s_{25} - \sigma_5 s_{26} \\ -\sigma_6 s_{36} - \sigma_2 s_{35} & -\sigma_5 s_{36} - \sigma_1 s_{35} \\ -\sigma_6 s_{46} - \sigma_2 s_{45} & -\sigma_5 s_{46} - \sigma_1 s_{45} \end{bmatrix}$$

where

$$\sigma_1 = \frac{s_{64}\sigma_{10}}{\sigma_{11}} + \frac{s_{54}\sigma_9}{\sigma_{11}}$$
$$\sigma_2 = \frac{s_{63}\sigma_{10}}{\sigma_{11}} + \frac{s_{53}\sigma_9}{\sigma_{11}}$$
$$\sigma_3 = \frac{s_{62}\sigma_{10}}{\sigma_{11}} + \frac{s_{52}\sigma_9}{\sigma_{11}}$$
$$\sigma_4 = \frac{s_{61}\sigma_{10}}{\sigma_{11}} + \frac{s_{51}\sigma_9}{\sigma_{11}}$$
$$\sigma_5 = \frac{s_{64}\sigma_{13}}{\sigma_{11}} + \frac{s_{54}\sigma_{12}}{\sigma_{11}}$$
$$\sigma_6 = \frac{s_{63}\sigma_{13}}{\sigma_{11}} + \frac{s_{53}\sigma_{12}}{\sigma_{11}}$$
$$\sigma_7 = \frac{s_{62}\sigma_{13}}{\sigma_{11}} + \frac{s_{52}\sigma_{12}}{\sigma_{11}}$$
$$\sigma_8 = \frac{s_{61}\sigma_{13}}{\sigma_{11}} + \frac{s_{51}\sigma_{12}}{\sigma_{11}}$$
$$\sigma_9 = s_{88} - s_{66}s_{77}s_{88} + s_{66}s_{78}s_{87}$$
$$\sigma_{10} = s_{87} + s_{56}s_{77}s_{88} - s_{56}s_{78}s_{87}$$
$$\sigma_{11} = s_{56}s_{78} + s_{55}s_{88} + s_{66}s_{77} + s_{65}s_{87} - s_{55}s_{66}s_{77}s_{88} + s_{55}s_{66}s_{78}s_{87} + s_{56}s_{65}s_{77}s_{88} - s_{56}s_{65}s_{78}s_{87} - 1$$
$$\sigma_{12} = s_{78} + s_{65}s_{77}s_{88} - s_{65}s_{78}s_{87}$$
$$\sigma_{13} = s_{77} - s_{55}s_{77}s_{88} + s_{55}s_{78}s_{87}.$$

REFERENCES

[1] M. Mauerer, A. Tüysüz, and J. W. Kolar, "Low-jitter GaN E-HEMT gate driver with high common-mode voltage transient immunity," *IEEE Trans. Ind. Electron.*, vol. 64, no. 11, pp. 9043–9051, Nov. 2017.

[2] T. Kim, D. Feng, M. Jang, and V. G. Agelidis, "Common mode noise analysis for cascaded boost converter with silicon carbide devices," *IEEE Trans. Power Electron.*, vol. 32, no. 3, pp. 1917–1926, Mar. 2017.

[3] D. Han, C. T. Morris, W. Lee, and B. Sarlioglu, "A case study on common mode electromagnetic interference characteristics of GaN HEMT and Si MOSFET power converters for EV/HEVs," *IEEE Trans. Transp. Electrific.*, vol. 3, no. 1, pp. 168–179, Mar. 2017.

[4] D. Han, S. Li, Y. Wu, W. Choi, and B. Sarlioglu, "Comparative analysis on conducted CM EMI emission of motor drives: WBG versus Si devices," *IEEE Trans. Ind. Electron.*, vol. 64, no. 10, pp. 8353–8363, Oct. 2017.

[5] Z. Zhang, B. He, D. D. Hu, X. Ren, and Q. Chen, "Common mode noise modeling and reduction for 1-MHz eGaN multi-output DC–DC converters," *IEEE Trans. Power Electron.*, 2018.

[6] H. C. P. Dymond *et al.*, "A 6.7-GHz active gate driver for GaN FETs to combat overshoot, ringing, and EMI," *IEEE Trans. Power Electron.*, vol. 33, no. 1, pp. 581–594, Jan. 2018.

[7] Y. Shi, Y. Zhang, L. Wang, and H. Li, "Reduction of EMI noise due to non ideal interleaving in a 100 kW SiC PV converter," *IEEE Trans. Power Electron.*, vol. 34, no. 1, pp. 13–19, Jun. 2019.

[8] L. Wang, Y. Shi, and H. Li, "Anti-EMI noise digital filter design for a 60-kW five-level SiC inverter without fiber isolation," *IEEE Trans. Power Electron.*, vol. 33, no. 1, pp. 13–17, Jan. 2018.

[9] A. Alam, M. K. Mukul, and P. Thakura, "Wavelet transform-based EMI noise mitigation in power converter topologies," *IEEE Trans. Electromagn. Compat.*, vol. 58, no. 5, pp. 1662–1673, Oct. 2016.

[10] C. K. Lee, D. Xu, B. M. H. Pong, S. Kiratipongvoot, and W. M. Ng, "A three-winding common mode inductor," *IEEE Trans. Power Electron.*, vol. 32, no. 7, pp. 5180–5187, Jul. 2017.

[11] S. Ohn, X. Zhang, R. Burgos, and D. Boroyevich, "Differential and common mode coupled inductor for parallel three-phase AC–DC converters," *IEEE Trans. Power Electron.*, 2018.

[12] D. Han, C. T. Morris, W. Lee, and B. Sarlioglu, "Comparison between output CM chokes for SiC drive operating at 20- and 200-kHz switching frequencies," *IEEE Trans. Ind. Appl.*, vol. 53, no. 3, pp. 2178–2188, May/Jun. 2017.

[13] D. O. Boillat, F. Krismer, and J. W. Kolar, "EMI filter volume minimization of a three-phase, three-level T-type PWM converter system," *IEEE Trans. Power Electron.*, vol. 32, no. 4, pp. 2473–2480, Apr. 2017.

[14] M. H. Hedayati and V. John, "Novel integrated CM inductor for single-phase power converters with reduced EMI," *IEEE Trans. Ind. Appl.*, vol. 53, no. 2, pp. 1300–1307, Mar./Apr. 2017.

[15] X. Shang, D. Su, H. Xu, and Z. Peng, "A noise source impedance extraction method for operating SMPS using modified LISN and simplified calibration procedure," *IEEE Trans. Power Electron.*, vol. 32, no. 6, pp. 4132–4139, Jun. 2017.

[16] C. Henglin, F. Limin, C. Wei, and Q. Zhaoming, "Modeling and measurement of the impedance of common mode noise source of switching converters," in *Proc. 21st Annu. IEEE Appl. Power Electron. Conf. Expo.*, 2006, p. 4.

[17] J. Deng and K. Y. See, "In-circuit characterization of common-mode chokes," *IEEE Trans. Electromagn. Compat.*, vol. 49, no. 2, pp. 451–454, May 2007.

[18] Z. Dongbing, D. Y. Chen, M. J. Nave, and D. Sable, "Measurement of noise source impedance of off-line converters," *IEEE Trans. Power Electron.*, vol. 15, no. 5, pp. 820–825, Sep. 2000.
[19] J. Meng, W. Ma, Q. Pan, J. Kang, L. Zhang, and Z. Zhao, "Identification of essential coupling path models for conducted EMI prediction in switching power converters," *IEEE Trans. Power Electron.* , vol. 21, no. 6, pp. 1795–1803, Nov. 2006.
[20] V. Tarateeraseth, H. Bo, S. Kye Yak, and F. G. Canavero, "Accurate extraction of noise source impedance of an SMPS under operating conditions," *IEEE Trans. Power Electron*, vol. 25, no. 1, pp. 111–117, Jan. 2010.
[21] C. Domínguez-Palacios, J. Bernal, and M. M. Prats, "Characterization of common mode chokes at high frequencies with simple measurements," *IEEE Trans. Power Electron.*, vol. 33, no. 5, pp. 3975–3987, May 2018.
[22] Y. Zhang, Y. Shi, and H. Li, "EMI noise separation method for three-phase WBG inverters with low sensitivity to parasitic parameters," *IEEE Trans. Power Electron.*, vol. 33, no. 6, pp. 4589–4593, Jun. 2018.
[23] A. Ales, J. L. Schanen, D. Moussaoui, and J. Roudet, "Impedances identification of DC/DC converters for network EMC analysis," *IEEE Trans. Power Electron.*, vol. 29, no. 12, pp. 6445–6457, Dec. 2014.
[24] C. Domínguez-Palacios, J. B. Mendez, and M. A. M. Prats, "Characterization of three-phase common-mode chokes at high frequencies," *IEEE Trans. Power Electron.*, vol. 33, no. 5, pp. 6471–6475, May 2018.
[25] T. Liu, T. T. Y. Wong, and Z. J. Shen, "A new characterization technique for extracting parasitic inductances of SiC power MOSFETs in discrete and module packages based on two-port s-parameters measurement," *IEEE Trans. Power Electron.*, vol. 33, no. 11, pp. 9819–9833, Nov. 2018.
[26] Agilent Technologies, "s-Parameter design (application note)," Palo Alto, CA, USA: Agilent, 2000.
[27] K. S. Kostov and J. J. Kyyra, "Insertion loss in terms of four-port network parameters," *IET Sci., Meas. Technol.*, vol. 3, pp. 208–216, 2009.
[28] J. R. Regue, M. Ribo, D. Duran, D. Badia, and A. Perez, "Common and differential mode characterization of EMI power-line filters from s-parameters measurements," in *Proc. Int. Symp. Electromagn. Compat.*, 2004, vol. 2, pp. 610–615.
[29] D. E. Bockelman and W. R. Eisenstadt, "Combined differential and common-mode scattering parameters: Theory and simulation," *IEEE Trans. Microw. Theory Techn.*, vol. 43, no. 7, pp. 1530–1539, Jul. 1995.
[30] G. Ting, D. Y. Chen, and F. C. Lee, "Separation of the common-mode- and differential-mode-conducted EMI noise," *IEEE Trans. Power Electron.*, vol. 11, no. 3, pp. 480–488, May 1996.
[31] *American National Standard Guide on the* Application *and* Evaluation *of EMI* Power-Line Filters *for* Commercial U*se*, ANSI C63.13-1991, 1991, p. 1.

Feng Zheng (S'06–M'08) received the B.S., M.S., and Ph.D degrees from Xi'an Jiaotong University, Xi'an, China, in 1993, 2004, and 2008, respectively, all in electrical engineering.

In 2008, he joined the School of Electrical and Mechanical Engineering, Xidian University, Xi'an. From 2010 to 2011, he was with the Center for Power Electronics Systems, Virginia Tech, Blacksburg, VA, USA, as a Postdoctoral Researcher. He then came back to Xidian University, where he is currently an Associate Professor. His research interests include electromagnetic compatibility, integrated magnetics, and power infrastructure of space solar power stations.

Wugang Wang received the bachelor's degree in electrical engineering and automation and the master's degree in electrical machinery and electrical appliances from Xidian University, Xi'an, China, in 2015 and 2018, respectively.

His main research interest includes electromagnetic compatibility.

Xiaofan Zhao received the B.S. degree from the North University of China, Taiyuan, China, in 1984.

From 2003 to 2018, she was the Director of the EMC Laboratory, China North Vehicle Research Institute, Beijing, China. Her research interest focuses on EMC issues in electric drive and new energy vehicle, including EMC principle, design technique, measurement method, and standard.

Mengke Cui received the B.S. degree in electrical engineering and automation from Xidian University, Xi'an, China, in 2016. He is currently working toward the M.S. degree with the School of Electrical and Mechanical Engineering, Xidian University.

Her main research interests include integrated magnetics and electromagnetic compatibility.

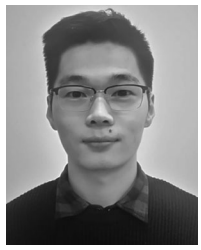

Qiang Zhang received the B.S. degree from Xidian University, Xi'an, China, in 2017. He is currently working toward the M.S. degree with the School of Electrical and Mechanical Engineering, Xidian University.

His main research interest includes electromagnetic compatibility.

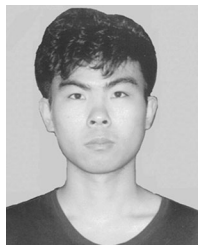

Guqing He received the B.S. degree from Xidian University, Xi'an, China, in 2018. He is currently working toward the M.S. degree with the School of Power Electronics Technology, Xidian University.

His main research interest includes electromagnetic compatibility.